



**Aerosol hygroscopic growth by active remote sensing and radiosoundings**

M. J. Granados-Muñoz  
et al.

This discussion paper is/has been under review for the journal Atmospheric Measurement Techniques (AMT). Please refer to the corresponding final paper in AMT if available.

# Hygroscopic growth of atmospheric aerosol particles based on active remote sensing and radiosounding measurements

M. J. Granados-Muñoz<sup>1,2</sup>, F. Navas-Guzmán<sup>1,2,\*</sup>, J. A. Bravo-Aranda<sup>1,2</sup>,  
J. L. Guerrero-Rascado<sup>1,2</sup>, H. Lyamani<sup>1,2</sup>, A. Valenzuela<sup>1,2</sup>, G. Titos<sup>1,2</sup>,  
J. Fernández-Gálvez<sup>1,2</sup>, and L. Alados-Arboledas<sup>1,2</sup>

<sup>1</sup>Dpt. Applied Physics, Faculty of Sciences, University of Granada, Fuentenueva s/n, 18071, Granada, Spain

<sup>2</sup>Andalusian Institute for Earth System Research (IISTA-CEAMA), Avda. del Mediterráneo s/n, 18006, Granada, Spain

\* now at: Institute of Applied Physics (IAP), University of Bern, Bern, Switzerland

Received: 14 September 2014 – Accepted: 22 September 2014 – Published: 10 October 2014

Correspondence to: M. J. Granados Muñoz (mjgranados@ugr.es)

Published by Copernicus Publications on behalf of the European Geosciences Union.

Title Page

Abstract

Introduction

Conclusions

References

Tables

Figures



Back

Close

Full Screen / Esc

Printer-friendly Version

Interactive Discussion



## Abstract

A new methodology based on combining active and passive remote sensing and simultaneous and collocated radiosounding data to study the aerosol hygroscopic growth effects on the particle optical and microphysical properties is presented. The identification of hygroscopic growth situations combines the analysis of multispectral aerosol particle backscatter coefficient and particle linear depolarization ratio with thermodynamic profiling of the atmospheric column. We analysed the hygroscopic growth effects on aerosol properties, namely the aerosol particle backscatter coefficient and the volume concentration profiles, using data gathered at Granada EARLINET station. Two study cases, corresponding to different aerosol loads and different aerosol types, are used for illustrating the potential of this methodology. Values of the aerosol particle backscatter coefficient enhancement factors range from  $2.10 \pm 0.06$  to  $3.90 \pm 0.03$ , being similar to those previously reported in the literature. Differences in the enhancement factor are directly linked to the composition of the atmospheric aerosol. The largest value of the aerosol particle backscatter coefficient enhancement factor corresponds to the presence of sulphate and marine particles that are more affected by hygroscopic growth. On the contrary, the lowest value of the enhancement factor corresponds to an aerosol mixture containing sulphates and slight traces of mineral dust. The Hänel parameterization is applied to these case studies, obtaining results within the range of values reported in previous studies, with values of the  $\gamma$  exponent of  $0.56 \pm 0.01$  (for anthropogenic particles slightly influenced by mineral dust) and  $1.07 \pm 0.01$  (for the situation dominated by anthropogenic particles), showing the convenience of this remote sensing approach for the study of hygroscopic effects of the atmospheric aerosol under ambient unperturbed conditions. For the first time, the retrieval of the volume concentration profiles for these cases using the Lidar Radiometer Inversion Code (LIRIC) allows us to analyse the aerosol hygroscopic growth effects on aerosol volume concentration, observing a stronger increase of the fine mode volume concentration with increasing relative humidity.

## Aerosol hygroscopic growth by active remote sensing and radiosoundings

M. J. Granados-Muñoz  
et al.

Title Page

Abstract

Introduction

Conclusions

References

Tables

Figures

◀

▶

◀

▶

Back

Close

Full Screen / Esc

Printer-friendly Version

Interactive Discussion



## 1 Introduction

The influence of atmospheric aerosols in the Earth's climate is still affected by a high uncertainty. Scientific knowledge on the interaction between atmospheric aerosol and solar radiation is quite low compared to other atmospheric constituents mainly due to atmospheric aerosol high spatio-temporal variability (IPCC, 2013). As it is well known, atmospheric aerosol can affect the Earth–Atmosphere energy budget by means of direct effects (by scattering or absorbing solar radiation) and indirect effects (mainly by changes in cloud properties). Therefore, changes in aerosol properties can highly influence the Earth's climate. Aerosol particles size may increase due to water uptake (hygroscopic growth) altering their size distribution and their associated optical and microphysical properties under high relative humidity conditions. Therefore, hygroscopic growth affects the direct scattering of radiation (Hänel, 1976; Hegg et al., 1996) and especially the indirect effects, as the affinity of atmospheric aerosols for water vapor is highly related to their ability to act as cloud condensation nuclei (CCN) (Charlson et al., 1992; Feingold and Morley, 2003).

In the past years there has been an increasing interest in the hygroscopic growth effects on the aerosol optical and microphysical properties and many studies have already been performed (e. g. Veselovskii et al., 2009; Zieger et al., 2013; Titos et al., 2014a, c). Much of the recent research was performed by means of humidified nephelometers (Covert et al., 1972; Fierz-Schmidhauser et al., 2010a, and references therein) or humidified tandem differential mobility analysers (Massling et al., 2007; Wu et al., 2013, and references therein). Nonetheless, these instruments present two main problems. Firstly, due to experimental set-up limitations it is difficult to provide accurate results above RH of 85 % (Wulfmeyer and Feingold, 2000). Secondly, they modify the ambient conditions by drying the air sample and then humidifying it again up to a certain value of RH, altering thus the aerosol properties and being also subject to aerosol losses in the sampling lines.

### Aerosol hygroscopic growth by active remote sensing and radiosoundings

M. J. Granados-Muñoz et al.

Title Page

Abstract

Introduction

Conclusions

References

Tables

Figures

◀

▶

◀

▶

Back

Close

Full Screen / Esc

Printer-friendly Version

Interactive Discussion







**Aerosol hygroscopic growth by active remote sensing and radiosoundings**M. J. Granados-Muñoz  
et al.

Title Page

Abstract

Introduction

Conclusions

References

Tables

Figures

◀

▶

◀

▶

Back

Close

Full Screen / Esc

Printer-friendly Version

Interactive Discussion



channel are detected, allowing us to study the depolarization properties of the atmospheric aerosol. Uncertainties associated to the elastic lidar signals are around 15 %, considering the statistical uncertainties retrieved with Monte Carlo techniques according to Pappalardo et al. (2004) and Guerrero-Rascado et al. (2008). The Raman lidar is part of EARLINET (Pappalardo et al., 2014). It has been part of the EARLINET-ASOS (European Aerosol Research Lidar Network – Advanced Sustainable Observation System) project and currently is included in the ACTRIS (Aerosols, Clouds, and Trace gases Research InfraStructure Network) European project.

In addition, the radiometric station is equipped with a sun photometer CIMEL CE-318-4. The sun photometer provides column-integrated atmospheric aerosol properties. The automatic tracking sun and sky scanning radiometer makes sun direct measurements with a 1.2° full field of view every 15 min at 340, 380, 440, 500, 675, 870, 940 and 1020 nm (nominal wavelengths). These solar extinction measurements are used to compute aerosol optical depth ( $\tau_\lambda$ ) at each wavelength except for the 940 nm channel, which is used to retrieve total column water vapour (or precipitable water). The estimated uncertainty in computed  $\tau_\lambda$ , due primarily to calibration uncertainty, is around 0.010–0.021 for field instruments (which is spectrally dependent, with the higher errors in the UV) (Eck et al., 1999). The sun photometer located in Granada is included in the AERONET network (Holben et al., 1998). The AERONET Version 2 Level 1.5 data are used in this study for the characterization of the aerosol properties and for the retrieval of the aerosol microphysical properties profiles in combination with backscattered elastic lidar signals by means of the Lidar Radiometer Inversion Code (LIRIC) (Chaikovskiy et al., 2012; Wagner et al., 2013; Granados-Muñoz et al., 2014).

For the analysis of the aerosol hygroscopic properties at the station, specific radiosounding launch campaigns are performed in order to obtain the RH humidity profiles since 2011. Radiosoundings (DFM-09 from GRAW Radiosondes) are launched simultaneously and collocated to the lidar measurements. They provide temperature (resolution 0.01 °C, accuracy 0.2 °C), pressure (resolution 0.1 hPa, accuracy 0.5 hPa), humidity (resolution 1 %, accuracy 2 %) and wind speed (resolution 0.1 m s<sup>-1</sup>, accuracy



532 nm ( $\beta$ -AE (355–532 nm)), related to the aerosol particles size, are also obtained. In addition, the particle linear depolarization ratio profiles ( $\delta_{532\text{nm}}^P$ ) are also calculated as explained in (Bravo-Aranda et al., 2013) in order to analyse variations in the shape of the particles.

5 The volume concentration profiles are retrieved by means of Lidar Radiometer Inversion Code (LIRIC). This algorithm provides vertical profiles of microphysical properties from a combined set of sun photometer and lidar data. LIRIC inputs are column-integrated optical and microphysical properties retrieved from the sun photometer measurements using AERONET code (Dubovik et al., 2006) and measured lidar elastic backscatter signals at three different wavelengths (355, 532, and 1064 nm). The depolarization information from lidar data can optionally be used. From this information, the volume concentration profiles for the fine and coarse mode are retrieved (distinguishing between coarse spherical and coarse spheroid particles if depolarization information is considered) (Chaikovsky et al., 2012; Wagner et al., 2013; Granados-Muñoz et al., 2014).

The RH profiles are directly measured by the radiosounding simultaneously and collocated to the lidar measurements, therefore no assumptions concerning the RH profile are needed as in previous studies (Ferrare et al., 1998; Wulfmeyer and Feingold, 2000; Feingold and Morley, 2003).

### 20 3.2 Procedure for selection of hygroscopic growth case studies

For the retrieval of aerosol hygroscopic properties from lidar data, very specific conditions need to be fulfilled. Aerosol water uptake is associated to the increase in aerosol optical properties such as the aerosol particle backscatter coefficient  $\beta_{\lambda}^P$  and aerosol particle microphysical properties such as the volume concentration. Therefore, for the study of hygroscopic properties, we need to observe an increase in the aerosol particle backscatter in a certain aerosol layer. This increase has to occur simultaneously to an increase in RH in this aerosol layer in order to consider hygroscopic growth as the possible cause of the changes in the aerosol particle properties. In addition,

## Aerosol hygroscopic growth by active remote sensing and radiosoundings

M. J. Granados-Muñoz et al.

Title Page

Abstract

Introduction

Conclusions

References

Tables

Figures

◀

▶

◀

▶

Back

Close

Full Screen / Esc

Printer-friendly Version

Interactive Discussion



## Aerosol hygroscopic growth by active remote sensing and radiosoundings

M. J. Granados-Muñoz  
et al.

Title Page

Abstract

Introduction

Conclusions

References

Tables

Figures

◀

▶

◀

▶

Back

Close

Full Screen / Esc

Printer-friendly Version

Interactive Discussion

a simultaneous decrease of the  $\beta$ -AE and the  $\delta_{532\text{nm}}^{\text{P}}$  is indicative of larger and more spherical particles, which is also clearly related to aerosol hygroscopic growth. To our knowledge, this is the first time that this simultaneous analysis of the  $\beta$ -AE and the  $\delta_{532\text{nm}}^{\text{P}}$  for evaluating hygroscopic growth is presented. This positive correlation between these two aerosol properties usually occur only in cases of aerosol hygroscopic growth or aging processes. Those cases fulfilling the previously described conditions are considered as potential cases of hygroscopic growth.

Once the potential cases of hygroscopic growth are detected, it is necessary to verify that in the analysed aerosol layer the atmospheric aerosol presents a certain degree of homogeneity. In this way, we can corroborate that the variations in the aerosol particle properties such as  $\beta_{\lambda}^{\text{P}}$ ,  $\beta$ -AE (355–532 nm),  $\delta_{532\text{nm}}^{\text{P}}$  and the volume concentration, are caused by the increase in the aerosol size due to water uptake and not to changes in the aerosol composition or load in the analysed layer. That means that the same aerosol type or mixture must be present along the analysed height range and almost no variations in the aerosol load must exist. For this purpose, ancillary information such as the backward trajectories of the air masses, the potential temperature profiles,  $\theta$ , or the water vapour mixing ratio profiles,  $r$ , are used to ensure that the aerosol layer under study is affected by hygroscopic growth. In this sense, if the origin and the trajectory of the air masses are independent of the altitude in the layer analysed, it is considered that the same aerosol type might have been advected and, therefore, a homogenous aerosol composition might be expected in the analysed layer. Otherwise, variations in the aerosol composition are expected and the case is not considered for analysis of hygroscopic growth. These air masses backward trajectories analyses are mainly used as a first approach selection criterion. In addition, good mixing is required as a boundary condition in order to guarantee the homogeneity of the atmospheric aerosol in the investigated layer. In general, constant profiles of  $\theta$  and  $r$  are indicators of well mixed conditions within the atmosphere. In our analysis,  $\theta$  and  $r$  are calculated in the analysed layer to check the mixing conditions. Both atmospheric variables are calculated from the radiosounding temperature and relative humidity profiles. Only those cases





show the potential of the technique described in Sect. 3.2. In these case studies, atmospheric conditions are highly supportive for aerosol hygroscopic growth at certain height ranges. A detailed analysis of these cases is presented in the following paragraphs.

Case I corresponds to the 22 July 2011. On this day, a radiosounding was launched at 20:30 UTC in coincidence with night-time lidar measurements. According to NAAPS model, 22 July 2011 at 18:00 UTC is characterized by the presence of mineral dust above Granada (Fig. S1a in the Supplement). A second case of hygroscopic growth is detected on 22 July 2013 (Case II) during the summer radiosounding campaign. For this specific day, the radiosounding was launched at 20:00 UTC in coincidence with simultaneous lidar measurements. On this day, NAAPS model indicates the presence of sulphates and smoke above the experimental site (Fig. S1b).

Sun photometer experimental data are also used for this analysis, since they provide information about the aerosol properties. In addition, sun photometer data are required for the retrieval of the volume concentration profiles with LIRIC. For Case I, sun photometer data suggest the presence of a Saharan dust plume that dissipates at late afternoon (Fig. 1a). The aerosol optical depth at 440 nm ( $\tau_{440\text{nm}}$ ) decreases during the afternoon, changing from 0.30 in the morning to values of 0.20 at 18:30 UTC. The Ångström exponent between 440 and 870 nm (AE (440–870 nm)) increases from 0.5 to 1.1, indicating an enhancement in the contribution of fine particles from 15:00 UTC. The aerosol size distributions retrieved during the day also indicate a decrease in the coarse mode and an increase of the fine mode from midday onwards. At 18:30 UTC (Fig. 1b) the aerosol size distributions indicate a balanced presence of both fine and coarse particles. This is confirmed by the fine mode fraction, determined through the SDA (spectral deconvolution algorithm, not shown) (O'Neill et al., 2003) that increases from 0.35 in the early morning up to 0.55 in the late evening. In the retrievals of single scattering albedo,  $\omega(\lambda)$ , corresponding to the morning hours it is observed a strong influence of mineral dust (high  $\omega(\lambda)$  values and increasing  $\omega(\lambda)$  with wavelength) (Fig. 1c). However, in the late afternoon,  $\omega(\lambda)$  values around 0.93, and its neutral spectral dependence

## Aerosol hygroscopic growth by active remote sensing and radiosoundings

M. J. Granados-Muñoz  
et al.

[Title Page](#)[Abstract](#)[Introduction](#)[Conclusions](#)[References](#)[Tables](#)[Figures](#)[◀](#)[▶](#)[◀](#)[▶](#)[Back](#)[Close](#)[Full Screen / Esc](#)[Printer-friendly Version](#)[Interactive Discussion](#)

**Aerosol hygroscopic growth by active remote sensing and radiosoundings**M. J. Granados-Muñoz  
et al.

Title Page

Abstract

Introduction

Conclusions

References

Tables

Figures

◀

▶

◀

▶

Back

Close

Full Screen / Esc

Printer-friendly Version

Interactive Discussion

suggest the presence in the atmospheric column of aerosol from anthropogenic origin with influence of residual mineral dust (Lyamani et al., 2006a, b; Valenzuela et al., 2012), which will be confirmed later with the lidar data and the backward trajectories analysis (Fig. 1c).

5 For the second case,  $\tau_{440\text{nm}}$  values indicate high aerosol loads reaching values above 0.40 at 17:19 UTC (Fig. 1d). The AE (440–870 nm) exhibits values larger than 1.2 during the whole day reaching 1.4 at 18:30 UTC, thus indicating a predominance of fine particles. The AERONET inversion retrievals during the whole day show bimodal size distributions with predominance of fine particles (Fig. 1e). Both, the  $\omega$  (440 nm) values close to 0.9, and their spectral dependence, with a decreasing trend with wave-  
10 length, evidence the presence of anthropogenic pollution and/or smoke over Granada (Lyamani et al., 2006a, b) (Fig. 1f), in agreement with NAAPS forecast model.

On both case studies, lidar measurements were running from 20:00 to 22:00 UTC. On 22 July 2011, lidar range corrected signal (RCS) time series (Fig. 2a) indicate the presence of atmospheric aerosol up to 3000 m a.s.l. Moreover, a strong increase of the RCS is observed in the height range around 2400 m a.s.l. between 20:30 and 21:00 UTC. On the other hand, the time series of the lidar RCS on 22 July 2013 (Fig. 2b) indicate that the atmospheric aerosol reach altitudes up to 3500 m a.s.l. with the strongest backscattered lidar signal around 3000 m a.s.l. For this second case,  
20 some clouds were observed from 21:30 UTC. The occurrence of these clouds might be related to the ability of hygroscopic aerosol to act as CCN.

The analysis of lidar data by means of the Klett–Fernald inversion algorithm for both cases is shown in Fig. 3. Mean profiles of  $\beta_{532\text{nm}}^{\text{P}}$ ,  $\beta\text{-AE}$  (355–532 nm) and  $\delta_{532\text{nm}}^{\text{P}}$  corresponding to the period 20:30–21:00 UTC for Case I and to 20:00–20:30 UTC for Case II are presented in this figure. On both cases, we observe a marked increase with altitude in  $\beta_{532\text{nm}}^{\text{P}}$ , in the range between 1330 and 2330 m a.s.l. for Case I and 1300 and 2700 m a.s.l. for Case II (Fig. 3a). Simultaneous to this increase in  $\beta_{532\text{nm}}^{\text{P}}$ , the RH also increases with altitude in both layers (Fig. 3b). Opposite to  $\beta_{532\text{nm}}^{\text{P}}$ ,  $\beta\text{-AE}$  (355–532 nm) decreases with altitude in both layers (Fig. 3c, Table 1). The decrease



## Aerosol hygroscopic growth by active remote sensing and radiosoundings

M. J. Granados-Muñoz  
et al.

Title Page

Abstract

Introduction

Conclusions

References

Tables

Figures

◀

▶

◀

▶

Back

Close

Full Screen / Esc

Printer-friendly Version

Interactive Discussion

levels considered (Fig. 4b) and they were travelling within the marine boundary layer before reaching Granada station, so they are likely loaded with marine aerosol from the Western Mediterranean Sea together with sulphates and smoke from Europe as indicated by the NAAPS model. The trajectories are very similar to those on Case I, but as for this case they travelled more slowly above the Mediterranean Sea they are likely loaded with more marine aerosol than in the previous case.

Vertical profiles of  $\theta$  and  $r$  measured with radiosounding data are also checked in order to corroborate good mixing conditions within the analysed aerosol layers. Both  $\theta$  and  $r$  profiles present almost constant values in the analysed layers in both case studies (Fig. 4c) and thus it can be inferred that the analysed layers are well mixed. Once these conditions are fulfilled, vertical homogeneity in the analysed layers can be assumed. Therefore, hygroscopic growth is foreseen for these cases since there is a high likelihood that changes in the aerosol properties are due to water uptake.

Therefore, according to all the previous results, these cases are considered representative of hygroscopic growth since there is an enhancement in  $\beta_{532\text{nm}}^{\text{P}}$  in coincidence with an increase in RH in the selected aerosol layers. In addition, the positive correlation between the  $\beta$ -AE (355–532 nm) and the  $\delta_{532\text{nm}}^{\text{P}}$  values suggests hygroscopic growth, since aerosol particles become larger and more spherical due to water uptake. Backward trajectories analysis with HYSPLIT and the height independency of  $\theta$  and  $r$  in the analysed height range corroborates that the enhancement of  $\beta_{532\text{nm}}^{\text{aer}}$  is due to water uptake because of the homogeneity of the aerosol layer.

Following the methodology described in Sect. 3.2, from the combination of the  $\beta_{532\text{nm}}^{\text{P}}$  and RH profiles in Fig. 3, the aerosol particle backscatter coefficient enhancement factor  $f_{\beta}(\text{RH})$  is obtained as indicated in Eq. (1).

In Case I,  $\text{RH}_{\text{ref}} = 60\%$ , which is the lowest value measured in the investigated layer. The dependence of  $f_{\beta}(\text{RH})$  with the RH is shown in the resultant humidogram in Fig. 5a. From this figure, it is evident that  $\beta_{532\text{nm}}^{\text{P}}$  increases 2.5 times ( $f_{\beta}(90\%) = 2.5$ ) in the range of humidity between 60 and 90%. The humidogram in Case II (Fig. 5b) shows that  $f_{\beta}(83\%) = 3.5$ , in the range of RH between 40 and 83%. For Case II,  $\text{RH}_{\text{ref}}$  is

established at 40 %, since it is the lowest RH value reached in the analysed layer for this case.

In a similar study performed by Veselovskii et al. (2009) in the East Coast of the United States, they got a value of the aerosol particle extinction coefficient enhancement factor  $f_{\alpha}(85\%) = 2.3$  in the presence of the typical continental haze using  $RH_{ref} = 60\%$ . It is necessary to take into account that Veselovskii et al. (2009) used the aerosol particle extinction coefficient profile and thus results are comparable only in a contextual way, since it would be necessary to know the influence of the aerosol hygroscopic growth on the aerosol particle lidar ratio to perform a quantitative comparison. For Case I, the value obtained here for  $f_{\beta}(85\%)$  is much lower than the one provided by Veselovskii et al. (2009) ( $f_{\beta}(85\%) = 1.5$ ). However, for Case II  $f_{\beta}(85\%) = 2.6$  using  $RH_{ref} = 60\%$ , which is very similar to the one obtained by Veselovskii et al. (2009).

A qualitative comparison with in-situ studies can be done in order to contextualize our results. However, when making this comparison it is necessary to take into account the differences between both techniques. In addition, in-situ analyses are usually performed under controlled conditions, whereas lidar data are measured under real and unperturbed conditions. Also, in-situ studies are frequently based on the retrieval of the aerosol particle light-scattering coefficient enhancement factor,  $f_{\sigma}(RH)$ , and not on the  $f_{\beta}(RH)$  used here. They usually provide values for  $f_{\sigma}(85\%)$  using  $RH_{ref}$  values of 40 % or lower (dry conditions). In order to compare our results to these in-situ studies using a  $RH_{ref}$  of 40 %, the Hänel parameterization is applied to our data in Case I (Fig. 5a). For Case II, the Hänel parameterization is necessary to obtain  $f_{\beta}(85\%)$ , since RH values above 83 % are not reached. Values of  $f_{\beta}(80\%)$ ,  $f_{\beta}(85\%)$  using  $RH_{ref} = 40\%$  and  $\gamma$  obtained are summarized for both cases in Table 2.

As it can be inferred from Table 2 and Fig. 5, the atmospheric aerosol presents a stronger hygroscopic growth for Case II. According to the experimental AERONET and lidar data and the ancillary information of the model, this may be due to the larger contribution of sulphates (in the fine mode) and marine aerosol (in the coarse mode) during Case II than during Case I in the analysed layers. In addition, a minor influence

**Aerosol hygroscopic growth by active remote sensing and radiosoundings**

M. J. Granados-Muñoz et al.

Title Page

Abstract

Introduction

Conclusions

References

Tables

Figures

◀

▶

◀

▶

Back

Close

Full Screen / Esc

Printer-friendly Version

Interactive Discussion





## Aerosol hygroscopic growth by active remote sensing and radiosoundings

M. J. Granados-Muñoz  
et al.

Title Page

Abstract

Introduction

Conclusions

References

Tables

Figures

◀

▶

◀

▶

Back

Close

Full Screen / Esc

Printer-friendly Version

Interactive Discussion



induce a significant overestimation of  $f_{VC}(RH)$ . Because of this,  $RH_{ref}$  for the fine mode is around 73%. The fine mode volume concentration presents a strong increase with RH, being  $f_{VC}(80\%) = 1.57$ . The total volume concentration smoothly increases with RH, mainly due to the increase in the fine mode ( $f_{VC}(80\%) = 1.16$  with  $RH_{ref} = 60\%$ ).

5 For case II, Fig. 6d shows  $f_{VC}(RH)$  vs. RH for the fine mode and the total volume concentration. It is observed an increase of  $f_{VC}(RH)$  with RH for the fine mode, slightly smoother than in the previous case, with  $f_{VC}(80\%) = 1.28$ . Using  $RH_{ref} = 60\%$  in order to make a comparison with Case I,  $f_{VC}(80\%)$  for Case II is 1.57 which is larger than in Case I. According to these results, the fine mode is the one dominating the hygroscopic growth in the analysed layers in both cases. Nonetheless, in Case II there is a larger increase of the total volume concentration with RH than in Case I, indicating that the coarse mode is more hygroscopic for Case II. This can be attributed to the higher influence of the marine aerosol advected from the Mediterranean Sea in the analysed layer in Case II and the minor influence of the residual mineral dust in the analysed layer in Case I, evidencing the influence of the chemical composition on the hygroscopic growth. Larger values of  $f(RH)$  are usually obtained for fine mode particles (Di Girolamo et al., 2012; Titos et al., 2014). In our study, it seems that the fine mode is clearly more dominated by more hygroscopic particles whereas the coarse mode is dominated by substances with very low hygroscopic growth, especially for Case I (possible influence of mineral dust in the aerosol mixture). Di Girolamo et al. (2012) observed similar behaviour analysing aged dust particles partially mixed with maritime, urban and organic aerosols. However, according to Zieger et al. (2013), the relative contribution of the fine and the coarse modes and the specific chemical composition for each mode are very important for determining  $f(RH)$ .

## 5 Conclusions

A new methodology to detect aerosol particle hygroscopic growth is implemented at Granada EARLINET experimental site. Aerosol hygroscopic properties are analysed









**Aerosol hygroscopic growth by active remote sensing and radiosoundings**M. J. Granados-Muñoz  
et al.

Title Page

Abstract

Introduction

Conclusions

References

Tables

Figures

◀

▶

◀

▶

Back

Close

Full Screen / Esc

Printer-friendly Version

Interactive Discussion



planetary boundary layer height using lidar: one-year analysis over southeastern Spain, *J. Geophys. Res.-Atmos.*, 117, D18208, doi:10.1029/2012JD017524, 2012.

Granados-Muñoz, M. J., Guerrero-Rascado, J. L., Bravo-Aranda, J. A., Navas-Guzmán, F., Valenzuela, A., Lyamani, H., Chaikovsky, A., Wandinger, U., Ansmann, A., Dubovik, O., Grudo, J. O., and Alados-Arboledas, L.: Retrieving aerosol microphysical properties by Lidar-Radiometer Inversion Code (LIRIC) for different aerosol types, *J. Geophys. Res.-Atmos.*, 119, 4836–4858, 2014.

Guerrero-Rascado, J. L., Ruiz, B., and Alados-Arboledas, L.: Multi-spectral Lidar characterization of the vertical structure of Saharan dust aerosol over southern Spain, *Atmos. Environ.*, 42, 2668–2681, 2008.

Guerrero-Rascado, J. L., Olmo, F. J., Avilés-Rodríguez, I., Navas-Guzmán, F., Pérez-Ramírez, D., Lyamani, H., and Alados Arboledas, L.: Extreme Saharan dust event over the southern Iberian Peninsula in september 2007: active and passive remote sensing from surface and satellite, *Atmos. Chem. Phys.*, 9, 8453–8469, doi:10.5194/acp-9-8453-2009, 2009.

Guerrero-Rascado, J. L., Andrey, J., Sicard, M., Molero, F., Comerón, A., Pujadas, M., and Alados-Arboledas, L.: Aerosol closure study by lidar, Sun photometry, and airborne optical counters during DAMOCLES field campaign at El Arenosillo sounding station, Spain, *J. Geophys. Res.-Atmos.*, 116, D02209, doi:10.1029/2010JD014510, 2011.

Hänel, G.: The properties of atmospheric aerosol particles as functions of the relative humidity at thermodynamic equilibrium with the surrounding moist air, in: *Advances in Geophysics*, edited by: Landsberg, H. E. and Mieghem, J. V., Elsevier, 73–188, 1976.

Hegg, D. A., Covert, D. S., Rood, M. J., and Hobbs, P. V.: Measurements of aerosol optical properties in marine air, *J. Geophys. Res.-Atmos.*, 101, 12893–12903, 1996.

Holben, B. N., Eck, T. F., Slutsker, I., Tanré, D., Buis, J. P., Setzer, A., Vermote, E., Reagan, J. A., Daufman, Y. J., Nakajima, T., Lavenu, F., Jankowiak, I., and Smirnov, A.: AERONET – a federated instrument network and data archive for aerosol characterization, *Remote Sens. Environ.*, 66, 1–16, 1998.

IPCC: Contribution of Working Group I to the Fifth Assessment Report of the Intergovernmental Panel on Climate Change, in: *Summary for Policymakers in Climate Change*, edited by: Stocker, T. F., Qin, D., Plattner, G. K., Tignor, M., Allen, S., Boschung, J., Nauels, A., Xia, Y., Bex, V., and Midgley, P., Cambridge University Press, 2013.

## Aerosol hygroscopic growth by active remote sensing and radiosoundings

M. J. Granados-Muñoz  
et al.

Title Page

Abstract

Introduction

Conclusions

References

Tables

Figures

◀

▶

◀

▶

Back

Close

Full Screen / Esc

Printer-friendly Version

Interactive Discussion



Kim, J., Yoon, S. C., Jefferson, A., and Kim, S. W.: Aerosol hygroscopic properties during Asian dust, pollution, and biomass burning episodes at Gosan, Korea in April 2001, *Atmos. Environ.*, 40, 1550–1560, 2006.

Klett, J. D.: Stable analytical inversion solution for processing lidar returns, *Appl. Optics*, 20, 211–220, 1981.

Klett, J. D.: Lidar inversion with variable backscatter/extinction ratios, *Appl. Optics*, 24, 1638–1643, 1985.

Landulfo, E., Papayannis, A., Artaxo, P., Castanho, A. D. A., de Freitas, A. Z., Souza, R. F., Vieira Junior, N. D., Jorge, M. P. M. P., Sánchez-Ccoyllo, O. R., and Moreira, D. S.: Synergetic measurements of aerosols over São Paulo, Brazil using LIDAR, sunphotometer and satellite data during the dry season, *Atmos. Chem. Phys.*, 3, 1523–1539, doi:10.5194/acp-3-1523-2003, 2003.

Lyamani, H., Olmo, F. J., Alcántara, A., and Alados-Arboledas, L.: Atmospheric aerosols during the 2003 heat wave in southeastern Spain I: spectral optical depth, *Atmos. Environ.*, 40, 6453–6464, 2006a.

Lyamani, H., Olmo, F. J., Alcántara, A., and Alados-Arboledas, L.: Atmospheric aerosols during the 2003 heat wave in southeastern Spain II: microphysical columnar properties and radiative forcing, *Atmos. Environ.*, 40, 6465–6476, 2006b.

Massling, A., Leinert, S., Wiedensohler, A., and Covert, D.: Hygroscopic growth of sub-micrometer and one-micrometer aerosol particles measured during ACE-Asia, *Atmos. Chem. Phys.*, 7, 3249–3259, doi:10.5194/acp-7-3249-2007, 2007.

Navas-Guzmán, F., Bravo-Aranda, J. A., Guerrero-Rascado, J. L., Granados-Muñoz, M. J., and Alados-Arboledas, L.: Statistical analysis of aerosol optical properties retrieved by Raman lidar over Southeastern Spain, *Tellus B*, 65, 21234, doi:10.3402/tellusb.v65i0.21234, 2013.

Navas-Guzmán, F., Fernández-Gálvez, J., Granados-Muñoz, M. J., Guerrero-Rascado, J. L., Bravo-Aranda, J. A., and Alados-Arboledas, L.: Tropospheric water vapour and relative humidity profiles from lidar and microwave radiometry, *Atmos. Meas. Tech.*, 7, 1201–1211, doi:10.5194/amt-7-1201-2014, 2014.

O'Neill, N. T., Eck, T. F., Smirnov, A., Holben, B. N., and Thulasirama, S.: Spectral discrimination of coarse and fine mode optical depth, *J. Geophys. Res.*, 108, 4559, doi:10.1029/2002JD002975, 2003.

Pahlow, M., Feingold, G., Jefferson, A., Andrews, E., Ogren, J. A., Wang, J., and Turner, D. D.: Comparison between lidar and nephelometer measurements of aerosol hygroscopicity at the



## Aerosol hygroscopic growth by active remote sensing and radiosoundings

M. J. Granados-Muñoz  
et al.

Title Page

Abstract

Introduction

Conclusions

References

Tables

Figures

◀

▶

◀

▶

Back

Close

Full Screen / Esc

Printer-friendly Version

Interactive Discussion



Titos, G., Lyamani, H., Cazorla, A., Sorribas, M., Foyo-Moreno, I., Wiedensohler, A., and Alados-Arboledas, L.: Study of the relative humidity dependence of aerosol light-scattering in southern Spain, *Tellus B*, 66, 24536, doi:10.3402/tellusb.v66.24536, 2014c.

Valenzuela, A., Olmo, F. J., Lyamani, H., Antón, M., Quirantes, A., and Alados-Arboledas, L.: Classification of aerosol radiative properties during African desert dust intrusions over south-eastern Spain by sector origins and cluster analysis, *J. Geophys. Res.-Atmos.*, 117, D06214, doi:10.1029/2011JD016885, 2012.

Veselovskii, I., Whiteman, D. N., Kolgotin, A., Andrews, E., and Korenskii, M.: Demonstration of aerosol property profiling by multiwavelength lidar under varying relative humidity conditions, *J. Atmos. Ocean. Tech.*, 26, 1543–1557, 2009.

Wagner, J., Ansmann, A., Wandinger, U., Seifert, P., Schwarz, A., Tesche, M., Chaikovsky, A., and Dubovik, O.: Evaluation of the Lidar/Radiometer Inversion Code (LIRIC) to determine microphysical properties of volcanic and desert dust, *Atmos. Meas. Tech.*, 6, 1707–1724, doi:10.5194/amt-6-1707-2013, 2013.

Wu, Z., Birmili, W., Poulain, L., Wang, Z., Merkel, M., Fahlbusch, B., van Pinxteren, D., Herrmann, H., and Wiedensohler, A.: Particle hygroscopicity during atmospheric new particle formation events: implications for the chemical species contributing to particle growth, *Atmos. Chem. Phys.*, 13, 6637–6646, doi:10.5194/acp-13-6637-2013, 2013.

Wulfmeyer, V. and Feingold, G.: On the relationship between relative humidity and particle backscattering coefficient in the marine boundary layer determined with differential absorption lidar, *J. Geophys. Res.-Atmos.*, 105, 4729–4741, 2000.

Zieger, P., Fierz-Schmidhauser, R., Weingartner, E., and Baltensperger, U.: Effects of relative humidity on aerosol light scattering: results from different European sites, *Atmos. Chem. Phys.*, 13, 10609–10631, doi:10.5194/acp-13-10609-2013, 2013.

## Aerosol hygroscopic growth by active remote sensing and radiosoundings

M. J. Granados-Muñoz  
et al.

**Table 1.** Values of the different aerosol properties at the lowest and highest altitudes of the analysed layers for Case I and Case II.

	Case I		Case II	
	1330 m.a.s.l.	2330 m.a.s.l.	1300 m.a.s.l.	2700 m.a.s.l.
$\beta_{532\text{nm}}^{\text{par}}$ ( $\text{Mm}^{-1} \text{sr}^{-1}$ )	2.17	4.20	1.11	3.84
RH (%)	60	90	40	85
$\beta$ -AE (355–532 nm)	1.3	0.8	2.0	1.0
$\delta_{532\text{nm}}^{\text{P}}$	0.10	0.05	0.07	0.03

[Title Page](#)
[Abstract](#)
[Introduction](#)
[Conclusions](#)
[References](#)
[Tables](#)
[Figures](#)
[◀](#)
[▶](#)
[◀](#)
[▶](#)
[Back](#)
[Close](#)
[Full Screen / Esc](#)
[Printer-friendly Version](#)
[Interactive Discussion](#)


## Aerosol hygroscopic growth by active remote sensing and radiosoundings

M. J. Granados-Muñoz  
et al.

**Table 2.** Values of  $f_{\beta}(80\%)$ ,  $f_{\beta}(85\%)$  and  $\gamma$  for the two cases of hygroscopic growth corresponding to the 22 July of 2011 and 2013, respectively. The uncertainties in  $f_{\beta}(\text{RH})$  are obtained by error propagation applied to Eq. (1). Only the uncertainty introduced by the aerosol particle backscatter coefficient is considered.

	Case I	Case II
$f_{\beta}(80\%)$	$1.60 \pm 0.03$	$3.00 \pm 0.02$
$\gamma$	$0.56 \pm 0.01$	$1.07 \pm 0.01$
$f_{\beta}(85\%)$	$2.10 \pm 0.06$	$3.90 \pm 0.03$

[Title Page](#)
[Abstract](#)
[Introduction](#)
[Conclusions](#)
[References](#)
[Tables](#)
[Figures](#)
[I◀](#)
[▶I](#)
[◀](#)
[▶](#)
[Back](#)
[Close](#)
[Full Screen / Esc](#)
[Printer-friendly Version](#)
[Interactive Discussion](#)

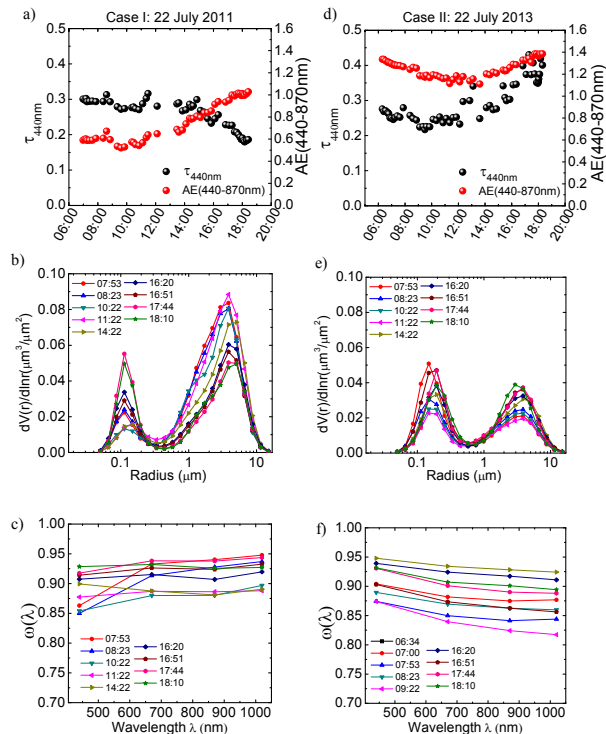


**Figure 1.** (a) AERONET  $\tau_{440}$  and AE (440–870) daily time series for Case I. (b) AERONET retrieved volume size distributions for Case I. (c)  $\omega(\lambda)$  for Case I. (d) AERONET  $\tau_{440}$  and AE (440–870) daily time series for Case II. (e) AERONET retrieved volume size distributions for Case II. (f)  $\omega(\lambda)$  for Case II.

Title Page

Abstract	Introduction
Conclusions	References
Tables	Figures

◀
▶

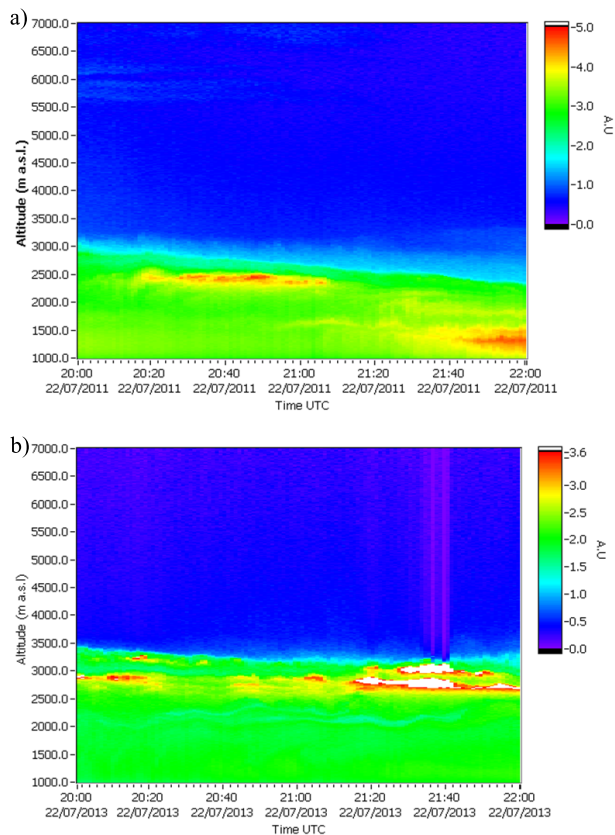
◀
▶

Back
 Close

Full Screen / Esc

Printer-friendly Version

Interactive Discussion

**Aerosol hygroscopic growth by active remote sensing and radiosoundings**M. J. Granados-Muñoz  
et al.

**Figure 2.** (a) Lidar RCS time series at 532 nm (arbitrary units) on 22 July 2011 from 20:00 to 22:00 UTC (b) Lidar RCS time series at 532 nm (arbitrary units) on 22 July 2013 from 20:00 to 22:00 UTC.

## Aerosol hygroscopic growth by active remote sensing and radiosoundings

M. J. Granados-Muñoz  
et al.

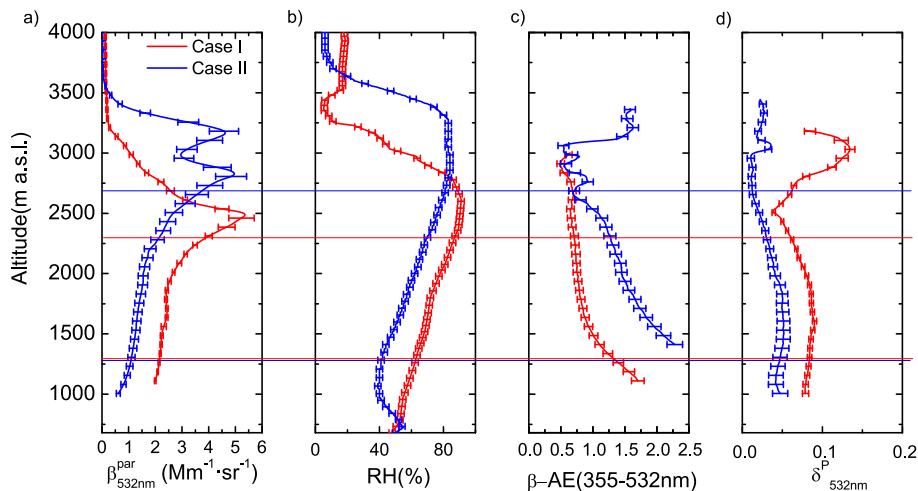


**Figure 3.** (a)  $\beta_{532\text{nm}}^{\text{P}}$  retrieved with Klett–Fernald algorithm (LR = 65 sr for Case I and LR = 70 for Case II) from 20:30 to 21:00 UTC on Case I and 20:00 to 20:30 UTC on Case II (b) RH profiles from the radiosounding launched at 20:30 UTC on Case I and at 20:00 UTC on Case II. (c)  $\beta\text{-AE}$  (355–532 nm) retrieved with Klett–Fernald algorithm for the same periods. (d)  $\delta_{532\text{nm}}^{\text{P}}$  retrieved from lidar data for the same periods. The error bars indicate the uncertainties calculated by Monte-Carlo technique. Horizontal lines represent the height limits of the aerosol layers selected for the analysis in Case I (red line) and Case II (blue lines).

## Aerosol hygroscopic growth by active remote sensing and radiosoundings

M. J. Granados-Muñoz et al.

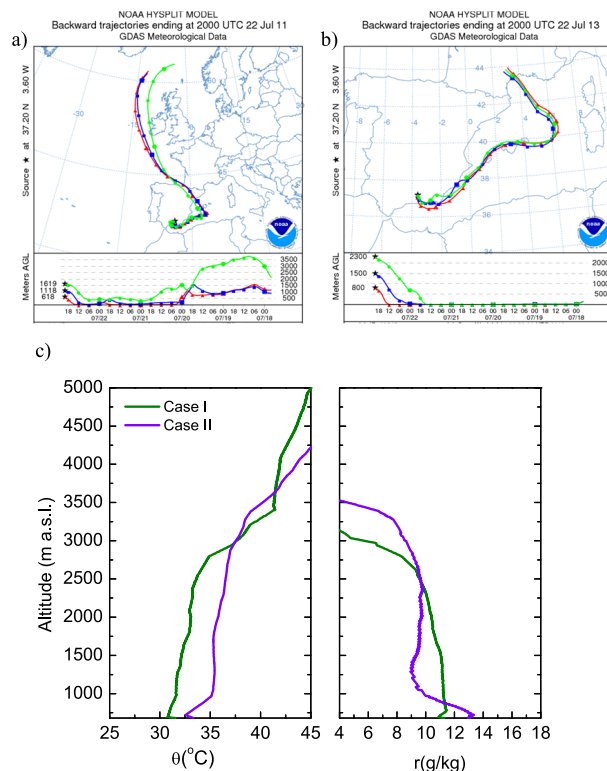


**Figure 4.** (a) 5 day backtrajectories of the air masses ending on 22 July 2011 at 20:00 UTC at Granada at 3 altitude heights within 1330–2330 m a.s.l. height range. (b) 5 day backtrajectories of the air masses ending on 22 July 2013 at 20:00 UTC at Granada at 3 altitude heights within 1300–2700 m a.s.l. height range. (c) Vertical profiles of  $\theta$  (in °C) and  $r$  (in  $\text{g kg}^{-1}$ ) from radiosounding data on 22 July 2011 at 20:30 UTC (Case I) and 22 July 2013 at 20:00 UTC (Case II).

## Aerosol hygroscopic growth by active remote sensing and radiosoundings

M. J. Granados-Muñoz  
et al.

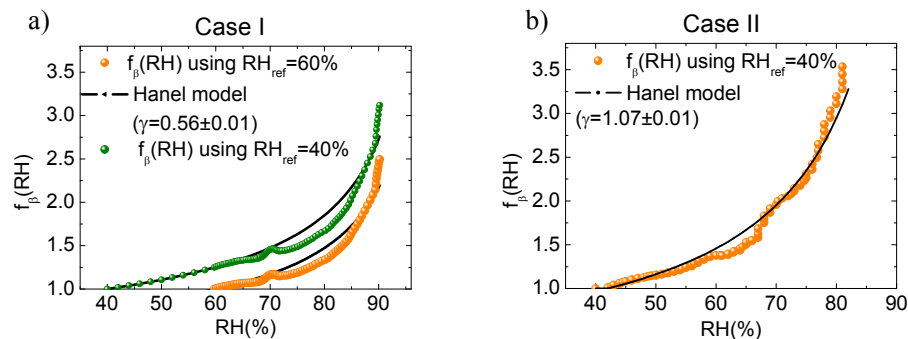


**Figure 5.** (a)  $f_{\beta}(\text{RH})$  retrieved on 22 July 2011 (Case I) from 20:30 to 21:00 UTC for the height range between 1330 and 2330 m a.s.l. (yellow dots for  $\text{RH}_{\text{ref}} = 60\%$  and green dots for  $\text{RH}_{\text{ref}} = 40\%$ ). (b)  $f_{\beta}(\text{RH})$  retrieved on 22 July 2013 (Case II) from 20:00 to 20:30 UTC for the layer corresponding to heights between 1300 and 2700 m a.s.l. using  $\text{RH}_{\text{ref}} = 40\%$ .

## Aerosol hygroscopic growth by active remote sensing and radiosoundings

M. J. Granados-Muñoz  
et al.

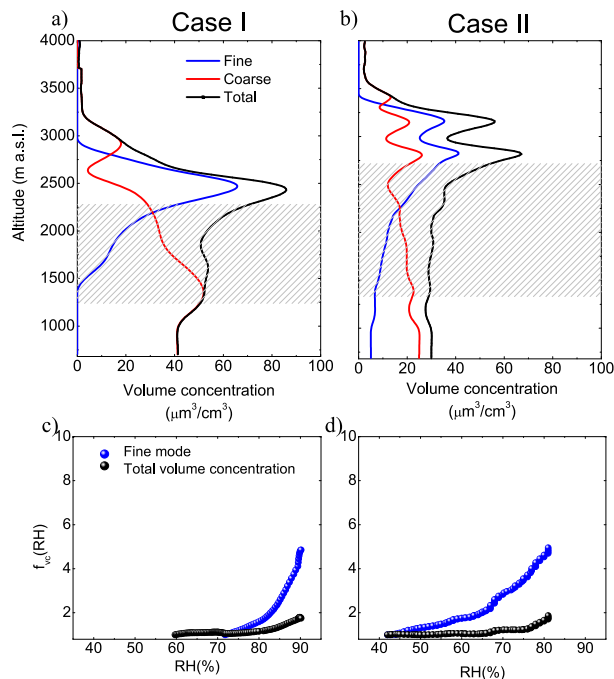


**Figure 6.** (a) LIRIC retrieved volume concentration (fine mode, coarse mode and total volume concentration) profiles on 22 July 2011 from 20:30 to 21:00 UTC. The shaded area indicates the height range where hygroscopic growth was investigated. (b) LIRIC retrieved volume concentration profiles on 22 July 2013 from 20:00 to 20:30 UTC. The shaded area indicates the investigated height range. (c)  $f_{VC}$ (RH) vs. RH for the fine mode and the total volume concentrations for 22 July 2011 and the layer corresponding to heights between 1330 and 2330 m a.s.l. (d)  $f_{VC}$ (RH) vs. RH for the fine mode and the total volume concentrations for 22 July 2013 and the layer corresponding to heights between 1300 and 2700 m a.s.l.